A Mg isotopic perspective on the mobility of magnesium during serpentinization and carbonation of the Oman ophiolite

Juan Carlos de Obeso[1], Danielle Priscilla Santiago Ramos[2], John Higgins[3], and Peter B Kelemen[1]

[1]Columbia University
[2]WHOI
[3]Princeton University

November 22, 2022

Abstract

Alteration of mantle peridotite in the Samail ophiolite forms secondary minerals, mainly serpentine and Mg-rich carbonates. Magnesium accounts for approximately 25 to 30% of peridotite mass and its mobility can be used to trace this alteration. We report the first set of Mg isotope measurements from peridotites and their alteration products in Oman. Partially serpentinized peridotites have Mg isotope ratios that are indistinguishable from estimates for the average mantle and bulk silicate earth (d26Mg =-0.25±0.04peridotite samples show large shifts in Mg isotopic composition. The range of d26Mg values for our suite of alteration products from the mantle section is ˜4.5the total range of terrestrial variability in d26Mg values. Serpentine veins are typically enriched in Mg (up to 0.96veins are associated with low Mg/Mg ratios (magnesite d26Mg =-3.3dolomite d26Mg =-1.91d26Mg values involves co-precipitation of serpentine and carbonates at water-to-rock ratios >10ˆ3. The coincidence of alteration products characterized by d26Mg values that are both lower and higher than bulk silicate Earth and the finite C ages of the carbonates suggest that both serpentinization and carbonation are ongoing in Oman. Rates of calcite precipitation in travertines inferred from D26Mgcal-fl suggest that travertine formation in Oman sequesters a total of 10ˆ6-10ˆ7 kg CO/yr, consistent with previous estimates.

A Mg isotopic perspective on the mobility of magnesium during serpentinization and carbonation of the Oman ophiolite

Juan Carlos de Obeso[1*], Danielle P. Santiago Ramos[2^], John A. Higgins[2], Peter B. Kelemen[3]

[1] Lamont Doherty Earth Observatory, Columbia University, Palisades, NY, USA

[2] Department of Geosciences, Princeton University, Princeton, NJ, USA

[3] Dept. of Earth & Environmental Sciences, Columbia University, Lamont Doherty Earth Observatory, Palisades, NY, USA

^ now at Geology & Geophysics, Woods Hole Oceanographic Institution, Wood Hole, MA, USA

*Corresponding author: Juan Carlos de Obeso (deobeso@ldeo.columbia.edu, jcdeobeso@gmail.com) Orcid: 0002-9962-8177

Key Points:

- The range of δ^{26}Mg from samples of the mantle section in the Oman ophiolite is ~4.5‰, or >60% of the total range of terrestrial variability.
- The range in δ^{26}Mg values involves co-precipitation of serpentine and carbonates at high water-to-rock ratios.
- Serpentinization and carbonation is ongoing in the mantle section of the Oman ophiolite.

(The above elements should be on a title page)

Abstract

Alteration of mantle peridotite in the Samail ophiolite forms secondary minerals, mainly serpentine and Mg-rich carbonates. Magnesium accounts for approximately 25 to 30% of peridotite mass and its mobility can be used to trace this alteration. We report the first set of Mg isotope measurements from peridotites and their alteration products in Oman. Partially serpentinized peridotites have Mg isotope ratios that are indistinguishable from estimates for the average mantle and bulk silicate earth (δ^{26}Mg =-0.25±0.04‰). However, more extensively altered peridotite samples show large shifts in Mg isotopic composition. The range of δ^{26}Mg values for our suite of alteration products from the mantle section is ~4.5‰, or >60% of the total range of terrestrial variability in δ^{26}Mg values. Serpentine veins are typically enriched in ^{26}Mg (up to 0.96‰) whereas Mg-carbonate veins are associated with low ^{26}Mg/^{24}Mg ratios (magnesite δ^{26}Mg =-3.3‰, dolomite δ^{26}Mg =-1.91‰). Our preferred explanation for the range in δ^{26}Mg values involves co-precipitation of serpentine and carbonates at water-to-rock ratios >10^3. The coincidence of alteration products characterized by δ^{26}Mg values that are both lower and higher than bulk silicate Earth and the finite ^{14}C ages of the carbonates suggest that both serpentinization and carbonation are ongoing in Oman. Rates of calcite precipitation in travertines inferred from $\Delta^{26}Mg_{cal\text{-}fl}$ suggest that travertine formation in Oman sequesters a total of 10^6-10^7 kg CO_2/yr, consistent with previous estimates.

1. Introduction

Alteration of ultramafic rocks is ubiquitous in near-surface environments, both on land and below the seafloor. Mantle olivine and pyroxene are unstable at near-surface conditions and undergo hydration (serpentinization) and carbonation when fluids are present (e.g. Moody, 1976).

These reactions result in the formation of serpentine minerals, carbonates, brucite, magnetite and other Fe-oxides and hydroxides. Serpentinization and carbonation reactions are often nearly isochemical apart from the addition of H_2O and CO_2 (e.g., Coleman & Keith 1971). Both observations and thermodynamic modeling suggest that changes in major element ratios such as Si/Mg are minor (e.g. ≤ 10% for low temperature reaction with seawater, Malvoisin, 2015, Figure 3; Monnier et al., 2006; Snow and Dick, 1995). However, other studies (e.g. Al-Khirbash, 2015; Auclair et al., 1993; Beinlich et al., 2018; de Obeso and Kelemen, 2018; Esteban Guzman et al., 2011; Hotz, 1964; Nasir et al., 2007; Skarpelis, 2006, de Obeso and Kelemen, 2020) have shown that under certain conditions mass transfer during serpentinization can lead to larger changes in major element chemistry. In Oman, while partially serpentinized harzburgites record a ~ 2% decrease in MgO/SiO_2 compared to the inferred composition of unaltered mantle peridotites (Monnier et al., 2006), there are examples of heavily altered harzburgite that have lost up to 30% of their original Mg (de Obeso and Kelemen, 2020).

Magnesium isotope studies show that the composition of the mantle and bulk silicate earth (BSE) is relatively uniform, with δ^{26}Mg values= -0.25±0.04‰ (2σ), (Teng, 2017; Teng et al., 2010). Liu et al. (2017) report δ^{26}Mg values of -0.12±0.13 ‰ (2σ) for altered seafloor peridotites. There are a limited number of studies on magnesium isotope compositions of ophiolite peridotites. Peridotites from the Purang ophiolite (Tibet) have δ^{26}Mg=-0.20±0.10‰ (2σ), within uncertainty of mantle compositions (Su et al., 2015), while peridotites from the Feragen and Linnajavri ultramafic bodies (Norway) have mantle-like Mg isotope ratios, with δ^{26}Mg values ranging from −0.35‰ to −0.23‰ (Beinlich et al., 2014).

Magnesium isotopes are known to fractionate during precipitation of carbonates and silicates from aqueous fluids. This fractionation can be used to constrain alteration processes during serpentinization and carbonation. Carbonates preferentially incorporate ^{24}Mg during crystallization, as observed in both experimental and natural samples, which yield large fractionation factors (Higgins and Schrag, 2010; Li et al., 2015; Mavromatis et al., 2013; Pearce et al., 2012; Shirokova et al., 2013; Tipper et al., 2006). On the other hand, available constraints on Mg fractionation factors associated with formation of serpentine polymorphs are equivocal. For example, based on dissolution experiments of San Carlos olivine at low temperature (~25ºC), Wimpenny et al., (2010) suggested that chrysotile preferentially removed light Mg from solution. In contrast, Ryu et al. (2016) synthetized lizardite from solution and reported that the mineral product was enriched in heavy Mg relative to the fluid at experimental temperatures of 90 and 250°C. Following a molecular dynamics approach, Wang et al. (2019) also concluded that lizardite crystallization preferentially removes ^{26}Mg from the fluid. These experimental results contrast with fractionation estimates based on natural samples that concluded that serpentinization does not fractionate Mg isotopes (Beinlich et al., 2014; Liu et al., 2017; Oskierski et al., 2019). Studies of natural samples also suggest that talc and Mg-rich clays formed during alteration are enriched in ^{26}Mg (Beinlich et al., 2014; Liu et al., 2017). In summary, whereas carbonate/water fractionation factors are large, those for serpentine are uncertain but close to 1. Thus Mg isotopes should be sensitive to the conditions of serpentinization and carbonation. Under closed system or low-water-to-rock conditions we expect little variability in Mg isotopes but at high water-to-rock ratios the full Mg isotope fractionation between Mg carbonate and silicates can be expressed.

To explore the behavior of Mg and Mg isotopes during serpentinization and carbonation we present the first suite of Mg isotope analyses of bulk-rock samples and mineral separates from the Samail ophiolite in Oman. Our sample suite consists of 37 samples of harzburgites and dunites with different degrees of alteration, as well as products of peridotite alteration (silicates and carbonates). We find that while the Mg isotopic compositions of partially serpentinized Oman peridotites (average δ^{26}Mg= -0.25±0.14‰, 2σ) are indistinguishable from mantle values, serpentine and carbonate samples are ^{26}Mg-enriched (up to 0.96‰) and ^{26}Mg-depleted (up to -3.38‰), respectively, compared to average mantle. We explore different hypotheses to explain the co-occurrence of high δ^{26}Mg serpentines and low δ^{26}Mg carbonates and discuss results in the context of previously published ^{14}C analyses which indicate that serpentinization and carbonation are ongoing during weathering of the Samail ophiolite mantle section.

2. Geological background and sample selection

The Samail ophiolite in eastern Oman is the best-exposed section of oceanic crust and mantle in the world (Figure 1). The mantle section of the ophiolite is composed of highly depleted harzburgites together with ~5-15% dunite (Boudier and Coleman, 1981; Braun, 2004; Braun and Kelemen, 2002; Collier, 2012). These peridotites exhibit different degrees of alteration ranging from ~30% serpentinized in "fresh" rocks to instances of completely serpentinized (Godard et al., 2000; Monnier et al., 2006) and completely carbonated peridotites (Falk and Kelemen, 2015; Nasir et al., 2007; Stanger, 1985). There is substantial evidence that alteration occurred throughout the history of the ophiolite. δ^{18}O data suggest that some alteration occurred near the axis of the spreading center as seawater interacted with the Samail crust (Gregory and Taylor, 1981), while an internal ^{87}Sr/^{86}Sr isochron on listvenite (carbonated peridotite) shows that alteration continued

during obduction and emplacement (Falk and Kelemen, 2015). The presence of hyperalkaline springs, recently crystallized carbonate veins and highly reduced fluids and mineral assemblages indicates that alteration is ongoing (e.g. Chavagnac et al., 2013a, 2013b; Clark and Fontes, 1990; Coleman and Keith, 1971; Kelemen et al., 2011; Kelemen and Matter, 2008; Mervine et al., 2014; Monnin et al., 2011; Neal and Stanger, 1985; Streit et al., 2012).

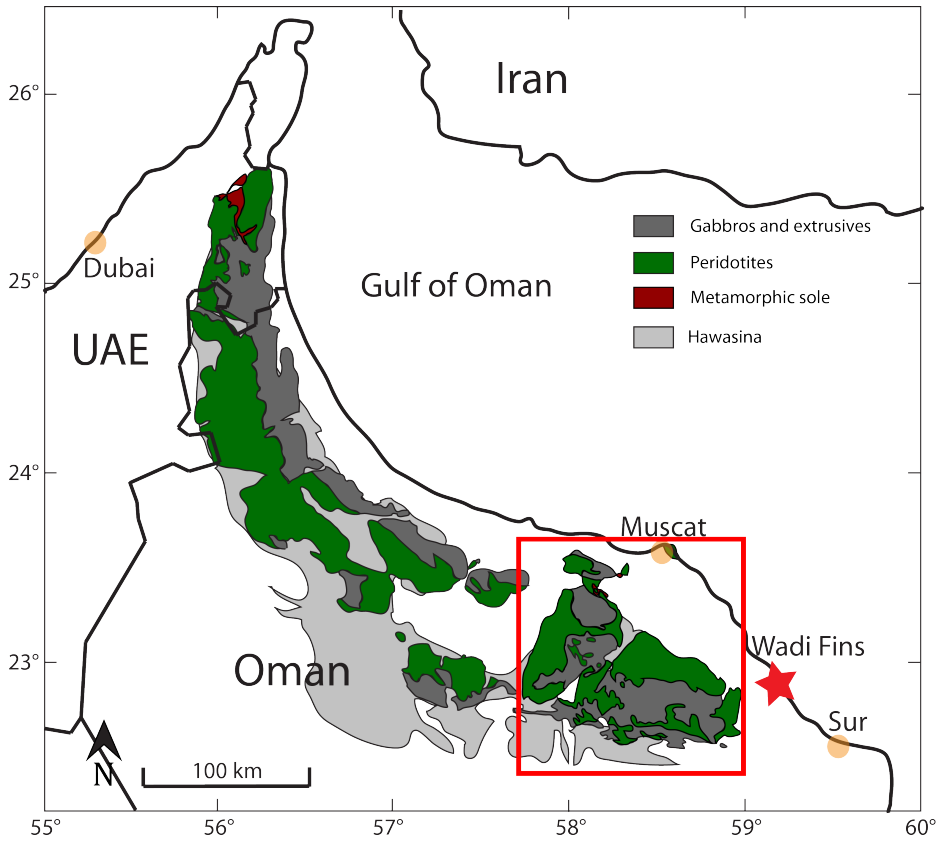

Figure 1. Simplified geologic map of the Samail ophiolite in Oman and the United Arab Emirates. All samples in this study come from the southern massifs (red square) and a small exposure beneath overlying Cretaceous to Eocene limestones at Wadi Fins (red star). Modified after (Nicolas et al., 2009).

Previous studies of low-temperature alteration of the Oman ophiolite propose that it occurs in three steps (e.g. Barnes et al., 1978, 1967; Barnes and O'Neil, 1969; Chavagnac et al., 2013a; Kelemen et al., 2011; Neal and Stanger, 1985; Noël et al., 2018; Paukert et al., 2012). Step 1 is

characterized by formation of Mg^{2+}-HCO_3^- rich fluids, as rain water dissolves Mg from peridotite and CO_2 from the atmosphere during near-surface weathering. During step 2, this so-called "Type I" water percolates deeper into peridotite leading to precipitation of Mg-rich carbonates, brucite and serpentine. These reactions remove carbon and Mg^{2+} from the fluid and dissolve Ca^{2+}, which is incompatible in the alteration minerals. The resulting fluids, known as "Type II" waters, have low Mg and C, high Ca and pH, and very low oxygen fugacities (Bruni et al., 2002; Clark and Fontes, 1990; Neal and Stanger, 1983; Paukert et al., 2012). During step 3, hyperalkaline "Type II" fluids are returned to the surface, where disequilibrium with the atmosphere leads to rapid uptake of atmospheric CO_2 and precipitation of calcite to form travertine deposits (Chavagnac et al., 2013a; Clark and Fontes, 1990; Kelemen et al., 2011; Kelemen and Matter, 2008; Mervine et al., 2014; Neal and Stanger, 1985; Paukert et al., 2012).

Magnesium fluxes during these three stages of alteration remain poorly constrained but inferences of water/rock during alteration have been made for Oman peridotites. Sulfides and in some cases native metals recording low oxygen fugacity observed in partially serpentinized peridotites are associated with low water/ratios (W/R) and incipient serpentinization (de Obeso and Kelemen, 2020; Frost, 1985; Kelemen et al., 2020; Lorand, 1988). Increased W/R are inferred from changes in accessory sulfide minerals (de Obeso and Kelemen, 2020) and the occurrence of diffuse carbonate vein networks in the peridotites (Noël et al., 2018). Even higher W/R are expected to have been involved in the formation of massive carbonate-serpentine veins which acted as main fluid paths for fluids interacting with peridotites (de Obeso and Kelemen, 2018; Noël et al., 2018). Secondary minerals from the three steps formed at variable W/R have different aqueous Mg^{2+}-mineral fractionation properties with silicates expected to become enriched in ^{26}Mg

and carbonates enriched in ^{24}Mg (e.g. Beinlich et al., 2014; Gao et al., 2018; Liu et al., 2017; Pinilla et al., 2015; Wang et al., 2019; Wimpenny et al., 2014) suggesting that Mg isotopes can be used as tracers of alteration.

All samples analyzed here were collected from the southern massifs of the ophiolite, within its mantle section (Figure 1). Previously described samples analyzed for this study can be separated into silicate- and carbonate-bearing groups. Silicate samples include relatively fresh harzburgites (n=6, average ~ 40% relict mantle minerals) and dunites (n=4, ~23%) from Hanghøj et al. (2010), highly serpentinized harzburgites (n=2, 37 and 14%) and dunites (n=1, 0%) from de Obeso and Kelemen (2018), and a set of serpentinized harzburgites (n=3, ~40%), high-Si harzburgite (n=3, 0%) and oxidized harzburgite (n=3, 0%) from de Obeso and Kelemen, 2020. We also include four samples not previously described: two serpentine veins, one serpentinite, and a "waxy vein" from a serpentinized body with Mg/Si~1.

Carbonate samples include two groups: completely carbonated peridotites, also known as listvenites, from Falk & Kelemen (2015), further classified as dolomite listvenites (n=2) and magnesite listvenites (n=2). We also analyzed massive carbonate veins from serpentinized peridotite outcrops, including two magnesite veins and one dolomite vein (Kelemen et al., 2011). The three carbonate vein samples have ^{14}C contents corresponding to ages of 32ka, 37ka, and 40ka (Kelemen et al., 2011). Two travertine samples from Kelemen et al. (2011) were also analyzed. These travertines are composed mainly of calcite, with ^{14}C contents corresponding to ages of 1630 and 18,450 years. We also include two carbonate vein samples not previously described: a massive

magnesite vein and a huntite vein. Major element compositions and locations for the new samples are reported in table S1.

3. Methods

Samples not previously described (4 silicates and 2 carbonates) were processed in Lamont Doherty Earth Observatory (LDEO). Samples were chipped using a jaw crusher and powdered using an alumina puck mill. Major element analyses and loss on ignition (LOI) were performed using an Agilent 720 Axial ICP-OES calibrated with rock standards (Table S2) following dissolution by lithium metaborate fusion and nitric acid.

For Mg isotopic analyses powders of all 37 samples and three USGS rock standards (BCR-2, BHVO-2, BIR-1A) were digested using a HNO_3:HF (3:1) digestion procedure at LDEO. Sample OM17-magnesite was processed in multiple digestion batches to check reproducibility (n=5). Once digested, < 1 μg of Mg from each sample was purified from the silicate/carbonate matrix using a Thermo Dionex 5000+ ion chromatography (IC) system at Princeton University. The procedure for both carbonate and silicate minerals is described in more detail in Husson et al. (2015) and Santiago Ramos et al. (2020)

Isotopic analyses were carried out at Princeton University on a Thermo Fisher Scientific Neptune Plus MC-ICP-MS. Standard-sample-standard bracketing was used to correct for instrumental mass fractionation (Galy et al., 2001) and values were normalized to an internal standard (DSM-3). Magnesium isotope ratios are reported using delta notation. Long-term external reproducibility is estimated by comparing Mg standard Cambridge-1 against DSM-3 standard.

Measured δ^{26}Mg values for Cambridge-1 yield an average of -2.59 ± 0.05‰ (2σ, n= 7), indistinguishable from the published value of -2.62±0.03‰ (2σ) (Galy et al., 2003; Teng et al., 2015). Reported uncertainties for each sample depend on the number of times the sample has been separated and analyzed. For a single separation and analysis, we report the long-term external reproducibility of Cambridge-1 (δ^{26}Mg 2σ=±0.09‰). USGS standards ran as unknowns are reported in Table S3. For multiple chromatographic separations and analyses (n> 1) we report the standard error of the mean (SE). All analyzed samples fall on an isotopic mass-dependent fractionation line in three-isotope space with slope of 0.5196±0.0024 (R^2=0.9992), indistinguishable from the value of 0.5210 estimated for equilibrium fractionation (Young and Galy, 2004). Given the linear relationship in three-isotope space, we discuss only δ^{26}Mg values.

4. Results

Measured δ^{26}Mg and δ^{25}Mg values for the sample suite are presented in Table 1 and shown in Figure 2. The observed range for this study is ~4.6‰ (-3.4‰ to +1.2‰), or >60% of the observed variability in δ^{26}Mg values on Earth (~7.5‰, from -5.6‰ to +1.8‰; Teng, 2017), and include δ^{26}Mg values that are both higher than and lower than unaltered mantle peridotite.

Sample	Reference	Lithology	δ^{26}Mg	δ^{25}Mg	2σ/2SE	n
OM94-99	Hanghøj et al 2008	Dunite	-0.22	-0.11	0.09	1
OM94-52D*	Hanghøj et al 2008	Dunite	-0.25	-0.11	0.09	1
OM94-74D	Hanghøj et al 2008	Dunite	-0.32	-0.15	0.09	1
OM94-110*	Hanghøj et al 2008	Dunite	-0.17	-0.06	0.09	1
OM94-67	Hanghøj et al 2008	Harzburgite	-0.25	-0.12	0.09	1
OM94-103	Hanghøj et al 2008	Harzburgite	-0.22	-0.11	0.09	1
OM94-61	Hanghøj et al 2008	Harzburgite	-0.24	-0.09	0.09	1
OM94-98	Hanghøj et al 2008	Harzburgite	-0.20	-0.09	0.09	1
OM94-101	Hanghøj et al 2008	Harzburgite	-0.29	-0.16	0.09	1
OM94-52H	Hanghøj et al 2008	Harzburgite	-0.42	-0.22	0.09	1
OM13-19	De Obeso & Kelemen 2018	Harzburgite	-0.17	-0.09	0.09	1
OM13-2	De Obeso & Kelemen 2018	Harzburgite	-0.24	-0.14	0.09	1
OM13-4	De Obeso & Kelemen 2018	Dunite	-0.24	-0.09	0.09	1
OM15-5-4	De Obeso & Kelemen 2020	Harzburgite	-0.10	-0.07	0.09	1
OM15-6-4	De Obeso & Kelemen 2020	Harzburgite	-0.09	-0.03	0.09	1
OM15-7-4	De Obeso & Kelemen 2020	Harzburgite	-0.09	-0.07	0.09	1
OM15-5-3	De Obeso & Kelemen 2020	Oxidized harzburgite	0.94	0.49	0.09	1
OM15-6-3	De Obeso & Kelemen 2020	Oxidized harzburgite	0.86	0.46	0.09	1
OM15-7-3	De Obeso & Kelemen 2020	Oxidized harzburgite	0.77	0.41	0.09	1
OM15-6-2	De Obeso & Kelemen 2020	Altered harzburgite	0.74	0.38	0.09	1
OM15-7-2	De Obeso & Kelemen 2020	Altered harzburgite	0.74	0.40	0.09	1
OM15-5-2	De Obeso & Kelemen 2020	Altered harzburgite	0.70	0.37	0.09	1
OM13-15A	This Study	Serpentinite	0.17	0.08	0.09	1
OM15-5-5	This Study	Waxy vein	1.19	0.60	0.09	1
OM13-15B	This Study	Serpentine vein	0.45	0.20	0.09	1
OM13-17A WP	This Study	Serpentine vein	0.96	0.51	0.09	1
OM09-11	Falk and Kelemen 2015	Magnesite Listvenite	-0.33	-0.18	0.09	1
OM10-26	Falk and Kelemen 2015	Magnesite Listvenite	-0.33	-0.16	0.09	1
OM10-14	Falk and Kelemen 2015	Dolomite Listvenite	-1.46	-0.78	0.09	1
OM10-15	Falk and Kelemen 2015	Dolomite Listvenite	-0.89	-0.48	0.09	1
OM07-39	Streit et al. 2012	Massive magnesite vein	-3.14	-1.64	0.09	1
OM07-27	Streit et al. 2012	Massive dolomite vein	-1.91	-1.02	0.09	1
OM17 Magnesite	This study	Massive magnesite vein	-3.38	-1.77	0.01	5
OM07-18	Kelemen et al 2011	Travertine forming now	-1.14	-0.56	0.07	2
OM07-34A	Kelemen et al 2011	Old travertine	-0.89	-0.44	0.05	2
OM07-07	Kelemen et al 2011	Carbonate vein	-3.39	-1.75	0.09	1
BA1B 11-2 17-27 cm	This study from mineralogy	Huntite vein	-3.04	-1.57	0.09	1

2σ=long-term external reproducibility of Cambridge-1; applied to all samples that were run only once through column chemistry + Neptune (i.e. not replicated)
2SE=applied to samples that were replicated, that is, run through column chemistry + Neptune more than once

Table 1. Samples numbers, reference, lithology and Mg isotopic compositions

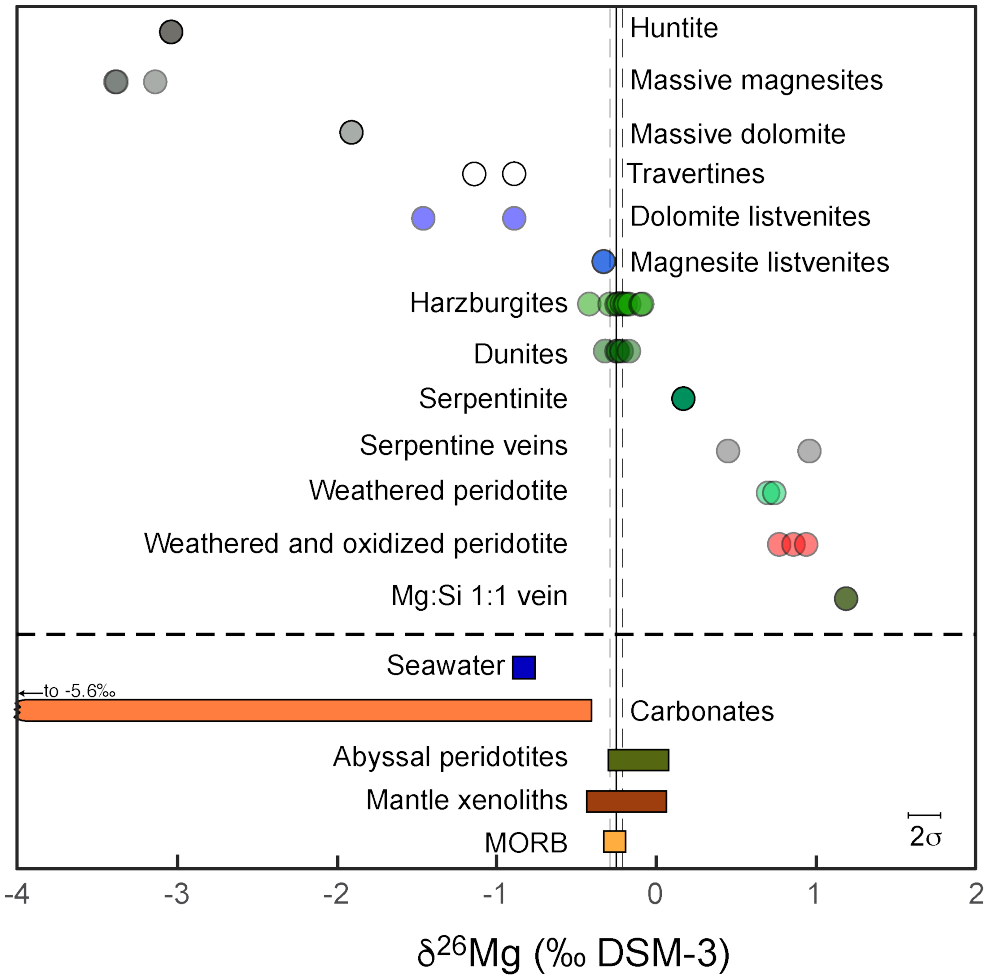

Figure 2. δ^{26}Mg for studied samples from the Oman ophiolite and selected terrestrial reservoirs (colored rectangles from Teng 2017). Black solid line represents the average mantle value, and vertical dashed black lines delineate the range of variability of mantle compositions from Teng (2010, 2017). Earth δ^{26}Mg range is ~7.5‰ (Teng, 2017)

Measured δ^{26}Mg values in partially serpentinized harzburgites and dunites are indistinguishable from the mantle (-0.25±0.14‰ (2σ) and -0.24±0.10‰ (2σ), respectively, Figure 3). Three samples from Wadi Fins (OM15-5-4, OM15-6-4 and OM15-7-4; de Obeso and Kelemen, 2020) are characterized by average δ^{26}Mg values higher than the mantle (-0.09±0.01‰, 2σ) are excluded from the harzburgite average as their compositions record significant Mg leaching (up to 30% in the most altered samples). Their completely hydrated (OM15-5-2, OM15-6-2 and OM15-7-2) and oxidized (OM15-5-3, OM15-6-3 and OM15-7-3) counterparts from the same outcrop are

characterized by higher δ^{26}Mg values (average of +0.73±0.04‰ for hydrated samples and +0.86±0.17‰ for oxidized samples, 2σ). Silicate mineral separates from veins in the Wadi Fins area are also characterized by δ^{26}Mg higher than the mantle. Two serpentine veins (OM13-17A WP and OM13-15B) have δ^{26}Mg values of +0.45‰ and +0.96‰ respectively, and a "waxy vein" (OM15-5-5) with molar Mg/Si of 1, composed of serpentine + stevensite or talc, has a δ^{26}Mg value of +1.19‰.

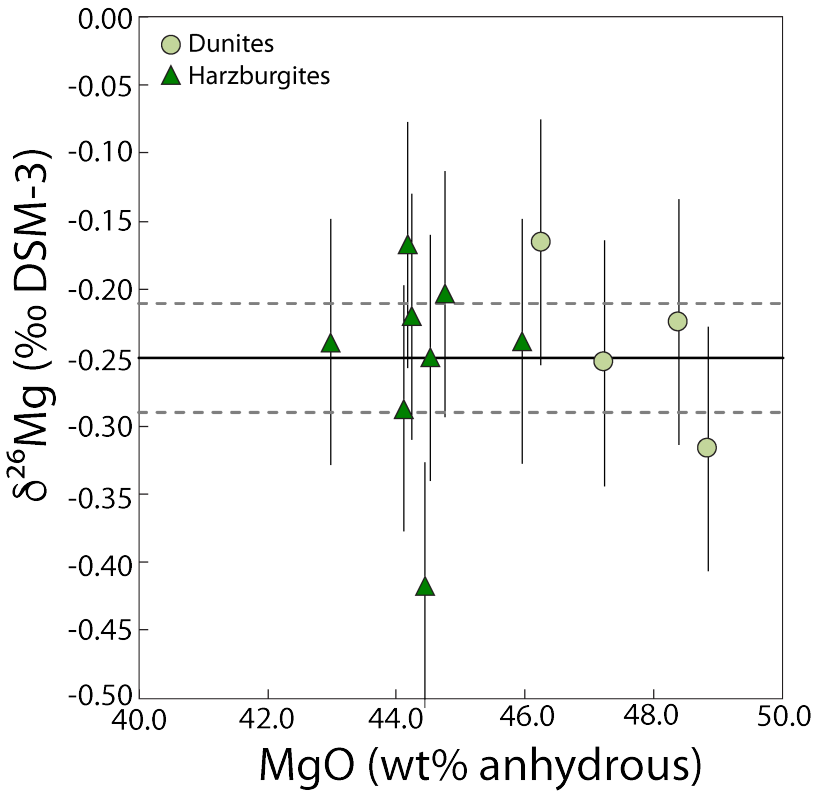

Figure 3. δ^{26}Mg (relative to DSM-3) vs. MgO (wt% anhydrous) for harzburgites and dunites. Black solid line represents the mantle average and dashed black lines encompass the range of mantle variability (Teng, 2017; Teng et al., 2010).

Measured δ^{26}Mg values in two magnesite listvenites (OM09-11 and OM10-26) are identical and indistinguishable from mantle values (-0.33‰), suggesting nearly isochemical carbonation as inferred from major element ratios by Falk and Kelemen (2015). In contrast, two

dolomite listvenites (OM10-14 and OM10-15) are characterized by lower δ^{26}Mg values, -1.46‰ and -0.89‰, respectively. Two massive magnesite veins (OM07-39, OM17 Magnesite) record δ^{26}Mg values of -3.14‰ and -3.39‰, or ~3‰ lower than the mantle. Dolomite (OM07-27) and huntite (BA1B 11-2 17-27cm) veins extracted from serpentinized peridotites are also characterized by low δ^{26}Mg values, -1.91‰ and -3.04‰, respectively. Finally, travertines with Mg-rich calcite (OM07-18 and OM07-34A) precipitated from Ca^{2+}-rich hyperalkaline springs (type II waters) are characterized by higher d^{26}Mg than the other carbonates (-1.14‰ and -0.89‰).

5. Discussion

5.1 δ^{26}Mg changes resulting from magnesium mobility

The degree of alteration of mantle peridotite can be assessed by looking at deviations from the mantle fractionation produced by melting and melt extraction in a MgO/SiO_2 vs Al_2O_3/SiO_2 plot (Figure 4). The mantle fractionation trend is a linear fit to theoretical and observed residues of mantle melting and melt extraction during adiabatic decompression beneath oceanic spreading ridges (Asimow, 1999; Baker and Beckett, 1999; Jagoutz et al., 1979). Based on deviations from the mantle fractionation trend, it is estimated that typical partially serpentinized harzburgites might have lost up to 2 wt% MgO on average (Monnier et al., 2006), though in some cases Si-gain can also lead to decreased MgO/SiO_2 ratios (de Obeso and Kelemen, 2018). Heavily weathered samples within 10 meters of a Cretaceous unconformity in Wadi Fins lost 30% of their initial Mg to the alteration fluid (de Obeso and Kelemen, 2020) and laterites along this unconformity elsewhere in Oman have lost even larger proportions of magnesium (Al-Khirbash, 2016, 2015). Nearly isochemical serpentinization of peridotite (other than H_2O addition) should preserve the

MgO/SiO_2 ratio of the original protolith, whereas deviations in all of our samples require Mg-loss (Snow and Dick, 1995) and/or Si-addition (de Obeso and Kelemen, 2018). This suggest that open system mass transfer of major elements has occurred during alteration (Figure 4).

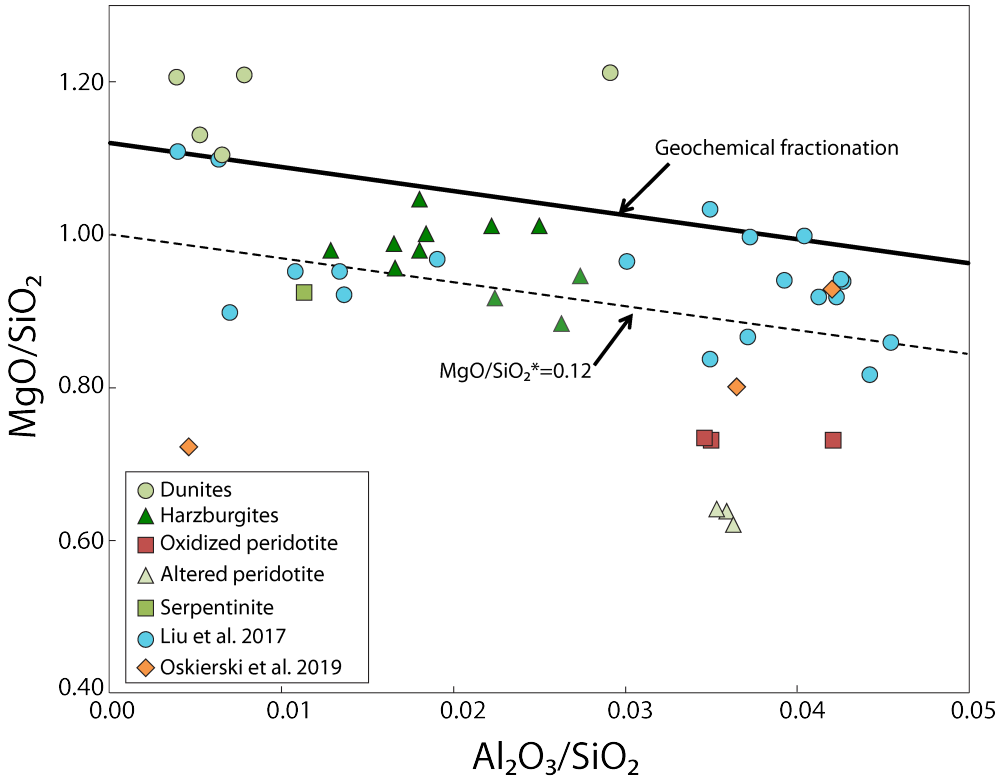

Figure 4. Whole rock MgO/SiO_2 vs Al_2O_3/SiO_2 showing sample deviations associated with peridotite alteration from the mantle fractionation trend (bold black line). The mantle fractionation trend is a linear fit to theoretical and observed residues of mantle melting and melt extraction during adiabatic decompression beneath oceanic spreading ridges (Asimow, 1999; Baker and Beckett, 1999). MgO/SiO_2*=0.12 shown as dashed black line.

Furthermore, the presence of meter-wide veins of magnesite in the Samail ophiolite mantle section provides additional evidence of Mg-mobility (Figure 5). However, the veins alone do not indicate if the Mg is derived by minor leaching from a large mass of peridotite, or extensive leaching from a smaller mass. Most analyzed magnesite, dolomite and calcite veins in Samail ophiolite peridotites record measurable ^{14}C, corresponding to ages less than ~ 50ka (Kelemen et

al., 2019, 2011; Kelemen and Matter, 2008; Mervine et al., 2014; Streit et al., 2012), suggesting that some of the alteration associated with Mg mobility is Pleistocene and Holocene.

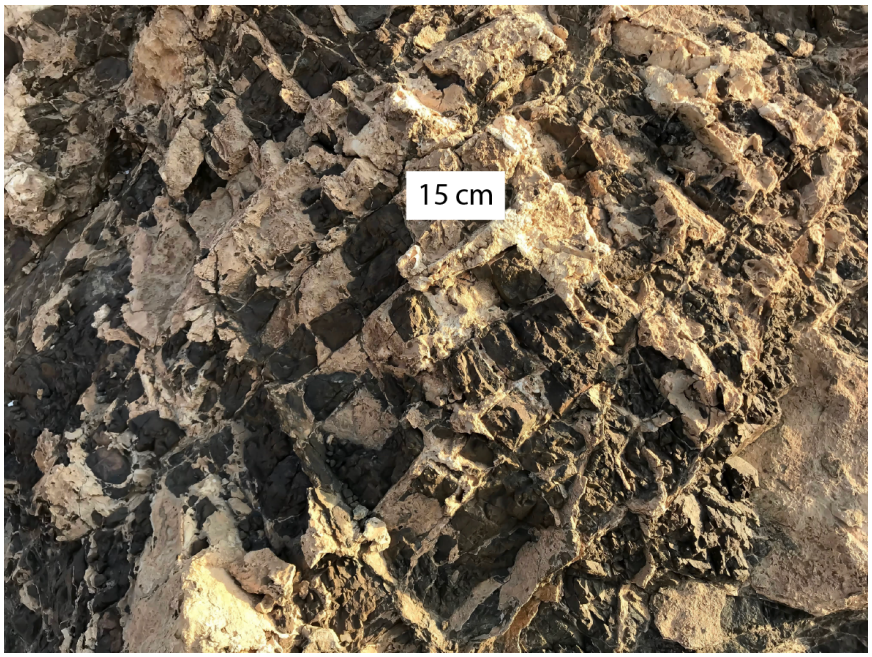

Figure 5. Massive magnesite veins containing angular blocks of serpentinized harzburgite in the Oman ophiolite (UTM 40Q E 671274 N 2536144).

In order to account for serpentinized harzburgite departures from the geochemical fractionation trend during alteration we use MgO/SiO_2* (Liu et al., 2017; Snow and Dick, 1995) defined as:

$$\left(\frac{MgO}{SiO_2}\right)^* = \left(-3.15 * \left(\frac{Al_2O_3}{SiO_2}\right)_{sample} + 1.12\right) - \left(\frac{MgO}{SiO_2}\right)_{sample}$$

All analyzed harzburgites in this study have $\left(\frac{MgO}{SiO_2}\right)^* > 0$ indicative of Mg-loss (Snow and Dick, 1995) and/or Si-addition (de Obeso and Kelemen, 2018) (Figure 5). Samples with $\left(\frac{MgO}{SiO_2}\right)^* <$

0.12 are partially serpentinized harzburgites with δ^{26}Mg indistinguishable from the Earth's mantle and BSE (δ^{26}Mg=0.25±0.04‰; Teng, 2017). As $\left(\frac{MgO}{SiO_2}\right)^*$ increases, whole rocks begin to deviate to heavier Mg isotope ratios (Figure 6). Samples with the highest $\left(\frac{MgO}{SiO_2}\right)^*$ in this study are the most enriched in ^{26}Mg and contain Mg-rich clays (de Obeso and Kelemen, 2020). These deviations suggest that 1) variable amounts of Mg have been leached from the peridotites depending on the degree of alteration at different W/R and 2) small Mg depletions are not reflected in δ^{26}Mg of the partially serpentinized harzburgites, which retain mantle-like Mg even at high degrees of serpentinization (e.g. OM13-2 and OM13-19).

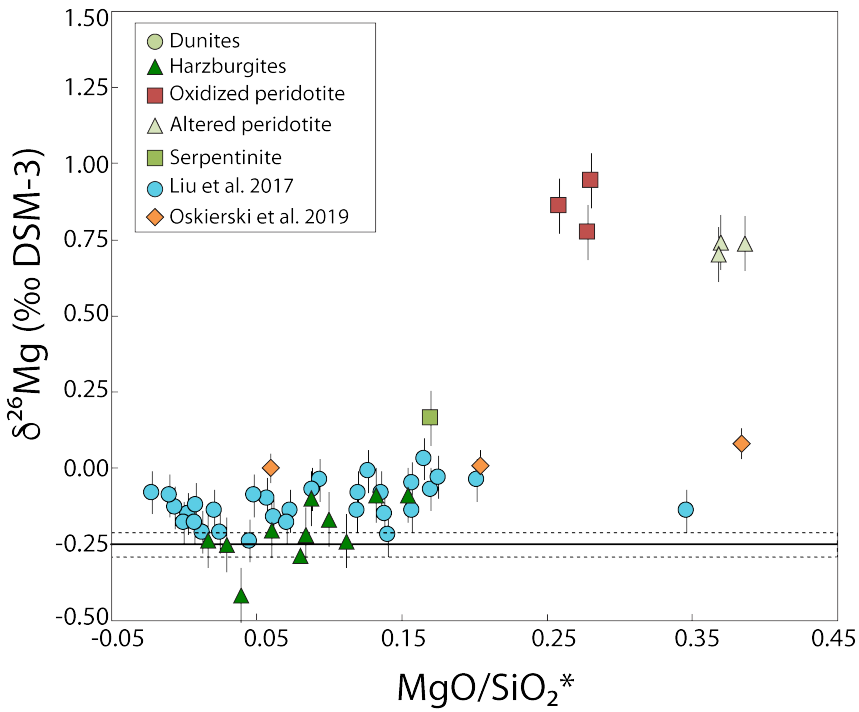

Figure 6. Bulk rock MgO/SiO_2* vs δ^{26}Mg for Oman samples, abyssal peridotites (Liu et al., 2017) and serpentinite (Oskierski et al. 2019). Black solid line is mantle average and dashed black lines delineate the range of variability of mantle compositions (Teng, 2017; Teng et al., 2010).

We associate the observed Mg mobility with the formation of alteration products in high W/R pathways, including serpentine and carbonates veins with δ^{26}Mg values that depart dramatically

from the canonical mantle value. In particular, Mg-carbonates have δ^{26}Mg between -0.64‰ and -3.14‰ lower than unaltered peridotite. Serpentine veins from Wadi Fins are depleted in Fe (Mg# 97-98) compared to ambient peridotite (Mg#90), and are interpreted to have formed at high water-to-rock ratios at temperatures between 25-60°C (de Obeso and Kelemen, 2018). Measured δ^{26}Mg values of these serpentine veins are up to 1.2‰ higher than unaltered peridotite. Little or no Mg-isotope fractionation, relative to mantle values, has been found in our whole rock samples of partially serpentinized peridotites, and in previous studies of similar lithologies (Beinlich et al., 2014; Liu et al., 2017). Thus, a different process for the formation of ^{26}Mg-enriched serpentine veins is required. Possibilities include 1) veins were enriched in ^{26}Mg due to isotopic fractionation associated with serpentine precipitation; 2) serpentine precipitated from a fluid enriched in ^{26}Mg due to the removal of ^{24}Mg in other alteration minerals (e.g. carbonates); or 3) some combination of 1) and 2).

5.2 Reaction path modeling

5.2.1 Model setup

To explore the hypothesis that elevated δ^{26}Mg values in serpentine veins are largely the consequence of precipitation from a high δ^{26}Mg fluid, formed by previous fractionation during crystallization of low ^{26}Mg carbonates, we developed a simple reactive transport model that simulates dissolution of primary minerals together with fractional crystallization of serpentine and carbonates based on the reaction path outlined by Barnes and O'Neil (1969) for serpentinization and carbonation systems and modelled by subsequent workers (Bruni et al., 2002; Paukert et al., 2012). We used Paukert et al., (2012) model that reproduces measured aqueous solute concentrations in the peridotite hosted springs via water rock interaction, including co-

precipitation of carbonates and serpentine. Most minerals associated with Mg mobility are modelled in the reaction path. This allows us to explore whether the evolution of Mg isotope compositions in alteration minerals during co-precipitation of carbonates and silicates is plausible and consistent with our data.

This model has three stages. In Stage I, rainwater in equilibrium with the atmosphere infiltrates the peridotite, forming chrysotile, calcite, hydromagnesite and magnetite. The fluid formed in stage I has an Mg^{2+}-HCO_3^- rich composition (Type I). In Stage II, Type I fluid reacts with fresh peridotite isolated from the atmosphere to form magnesium-rich carbonates, chrysotile and brucite, with the fluid evolving to Ca^{2+}-OH^- rich, Mg^{2+}-HCO_3^- poor compositions (Type II) until pH reaches 12 (maximum pH measured in the field). In Stage III (not explicitly modeled by Paukert et al., 2012), Type II fluids emerge on the surface and react with atmospheric CO_2 to form calcite. The model tracks the evolution of $\delta^{26}Mg$ in the resulting fluid and precipitated minerals during each stage. Important model variables and relevant references are given in Table 2. They include initial $\delta^{26}Mg$ fluid compositions, $Mg_{mineral\text{-}fluid}$ fractionation factors (α), and the temperature of alteration.

Model parameter	Value	Reference
Temperature	30°C	Weyhenmeyer et al., 2002
Magnesite $\alpha_{mgs\text{-}fluid}$	0.9972	Wang et al 2019
	0.9954	Schauble et al. 2011
	0.9979	Schott et al. 2016^
Dolomite $\alpha_{dol\text{-}fluid}$	0.9972	Wang et al. 2019
	0.9954	Schauble et al. 2011
	0.9979	Li et al. 2015
Hydromagnesite $\alpha_{hmgs\text{-}fluid}$	0.9990	Shirokova et al. 2013
Initial $\delta^{26}Mg$ fluid	-2.0‰	Teng, 2017
$[Mg]_0$ fluid	7.7×10^{-5} molal	Paukert et al. 2012
Peridotite $\delta^{26}Mg$	-0.25‰	Teng, 2017
[Mg] peridotite	28.4 wt%	Paukert et al. 2012

^ Schott is extrapolated from batch reaction data

Table 2. Model parameters

Equilibrium isotope fractionation of Mg isotopes is temperature dependent (Li et al., 2015; Pinilla et al., 2015; Ryu et al., 2016; Schott et al., 2016; Wang et al., 2019), rendering temperature estimates important for understanding alteration. For calculations in this paper, we used 30°C, approximately the current annual average temperature in the northern Oman mountains (Weyhenmeyer et al., 2002). This temperature is consistent with other constraints established in studies of most of the samples analyzed in this study. de Obeso and Kelemen (2018) estimated that alteration in Wadi Fins occurred between 25-60°C based on clumped isotope thermometry of carbonate veins in peridotite. Carbonate veins in typical, partially serpentinized mantle peridotites in the Samail ophiolite also yield crystallization temperatures between 25-50°C, calculated using both $\delta^{18}O$ exchange and clumped isotope thermometry (Kelemen et al., 2011; Streit et al., 2012).

Our model assumes that products of nearly isochemical, olivine serpentinization do not fractionate Mg isotopes from the fluid (α=1.0000 for serpentine and brucite) as concluded in previous studies of natural samples (Beinlich et al., 2014; Liu et al., 2017). The preferential incorporation of ^{24}Mg in carbonates, reported both in experimental and field observations (Higgins and Schrag, 2010; Li et al., 2015; Mavromatis et al., 2013; Pearce et al., 2012; Shirokova et al., 2013; Tipper et al., 2006), is a critical factor in our model. This isotopic fractionation is largely responsible for producing the fluid with high $\delta^{26}Mg$, that then produces serpentine veins with heavy Mg. We used carbonate-fluid fractionation factors (α) from empirical and experimental studies. For hydromagnesite, we used a fractionation factor of α=0.9990, derived from low temperature precipitation experiments on alkaline natural water of Salda Lake, Turkey (Shirokova et al., 2013). We prefer this value to the only other published value for hydromagnesite (Oelkers et al., 2018), because the latter group attributed their results to disequilibrium processes. For

magnesite and dolomite we used a range of fractionation factors reported in the literature, as listed in Table 2. Precipitation kinetics of magnesite and dolomite at low temperatures are poorly understood (Arvidson and Mackenzie, 1999; Saldi et al., 2012). Dolomite crystallization has not been achieved in laboratory conditions, even after a three decade long experiment (Land, 1998), and until 2017 magnesite had not been experimentally crystallized at temperatures below 60°C (e.g., Hänchen et al., 2008; Johnson et al., 2014), though more recent work produced magnesite at room temperature from fluids enriched in organic ligands (Power et al., 2017). In our models, magnesite-water fractionation factors at 30°C were extrapolated from higher temperature experiments (Li et al., 2015; Schott et al., 2016) or derived from first principles estimates and molecular dynamics (Schauble, 2011; Wang et al., 2019). Mg fractionation between calcite and fluid depends on multiple factors in addition to temperature (Li et al., 2012), including Mg content (Wang et al., 2019) and precipitation rate (Mavromatis et al., 2013). Fractionation factors for calcite are not directly used in the model.

The first two stages of the reaction path model yield calculated Mg isotope compositions of the fluid and precipitated minerals as a function of reaction progress, quantified using the water/rock ratio (W/R). We used the fractionation factors described above, and a model of assimilation and fractional crystallization (AFC) (DePaolo, 1981). The primary minerals (olivine, orthopyroxene and clinopyroxene) in the model have δ^{26}Mg of -0.25‰. At each step of the model, primary minerals are dissolved and secondary minerals (chrysotile + hydromagnesite in Stage I, chrysotile + brucite + dolomite and magnesite in Stage II) are allowed to precipitate. We assume that the starting Mg isotope composition in the fluid for the first stage is in equilibrium with the late Cretaceous to Eocene limestones that locally overlie the ophiolite, with initial $\delta^{26}Mg_{fluid}$ of -

2.0‰. Values for $\delta^{26}Mg_{fluid}$ at each model step are calculated using the AFC equation for stable isotopes:

$$\delta_f - \delta_f^0 = \left(\frac{r}{r-1}\right)\frac{C_a}{zC_f}\left[\delta_a - \delta_f^0 - \frac{D\Delta}{z(r-1)}\right]X(1-F^{-z}) - \frac{D\Delta}{(r-1)}lnF\left[1-\left(\frac{r}{r-1}\right)\frac{C_a}{zC_f}\right]$$

where δ_f and δ_a are the $\delta^{26}Mg$ of the fluid and the primary minerals respectively, $\Delta = 1000\ \ln\alpha_{mineral\text{-}fluid}$, r is the ratio of mass assimilated over mass precipitated, D is the bulk partition coefficient between secondary minerals and fluid, C_f is the Mg concentration in the fluid, C_a is the Mg concentration in the primary minerals, z=(r+D-1)/(r-1) and F is the ratio of fluid mass to initial fluid mass. $\Delta^{26}Mg$ of secondary minerals is calculated in each step using the fluid Mg isotope compositions and precipitated minerals fractionation factors ($\alpha_{mineral\text{-}fluid}$).

5.2.2 Model results

In Stage I, small extents of water-rock interaction (high W/R) cause fluid evolution from the initial $\delta^{26}Mg$ of -2‰ to a value of -0.25‰ (Figure 7). During precipitation of hydromagnesite, the fluid becomes slightly enriched in heavy isotopes before reaching a steady state at $\delta^{26}Mg$=-0.15‰ with W/R less than 100. The evolved fluid is Mg-HCO_3 rich.

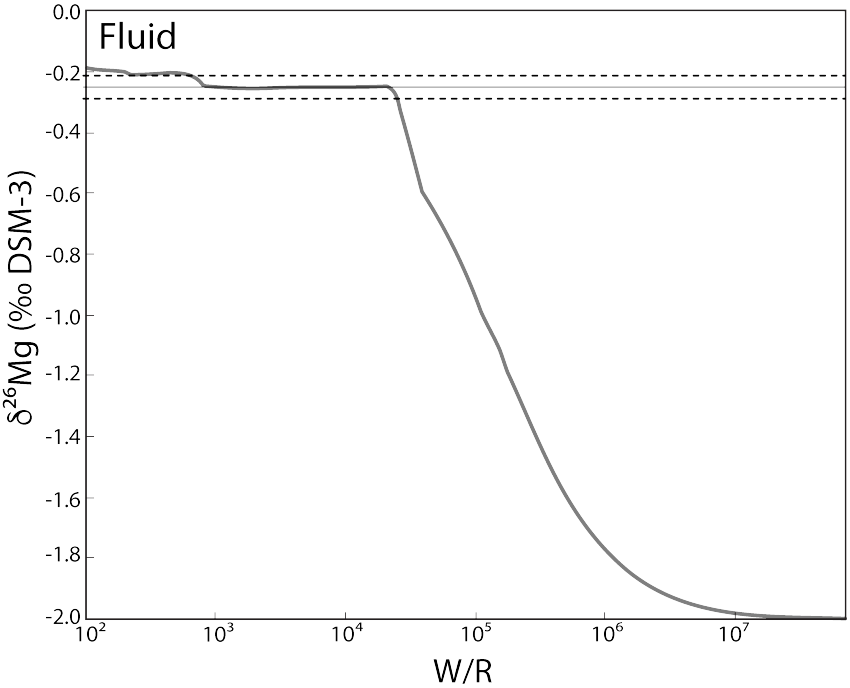

Figure 7. δ^{26}Mg evolution of the fluid in the first stage of reaction, open to gas exchange with the atmosphere. Black solid line is mantle average and dashed black lines delineate the range of variability of mantle compositions (Teng, 2017; Teng et al., 2010).

In Stage II, the Mg-HCO_3 rich fluid evolves to Mg- and C-depleted waters with high Ca^{2+} and pH as well as extremely low fO_2. Mineral precipitation is dominated by formation of magnesite and chrysotile with minor dolomite, at W/R between 2000-100,000 (Figure 8). Mg-rich carbonates begin to precipitate with their lightest δ^{26}Mg values, and evolve to heavier compositions as W/R decreases (Figure 8c and 8d). The precipitation of Mg-rich carbonates drives fluid and serpentine to heavier δ^{26}Mg (Figure 8b). Once the system becomes carbon-depleted, and magnesite disappears from the crystallizing mineral assemblage at W/R~1800, the fluid/serpentine system rapidly evolves to mantle-like isotope ratios (Figure 8b) while dolomite also disappears from the system (Figure 8d).

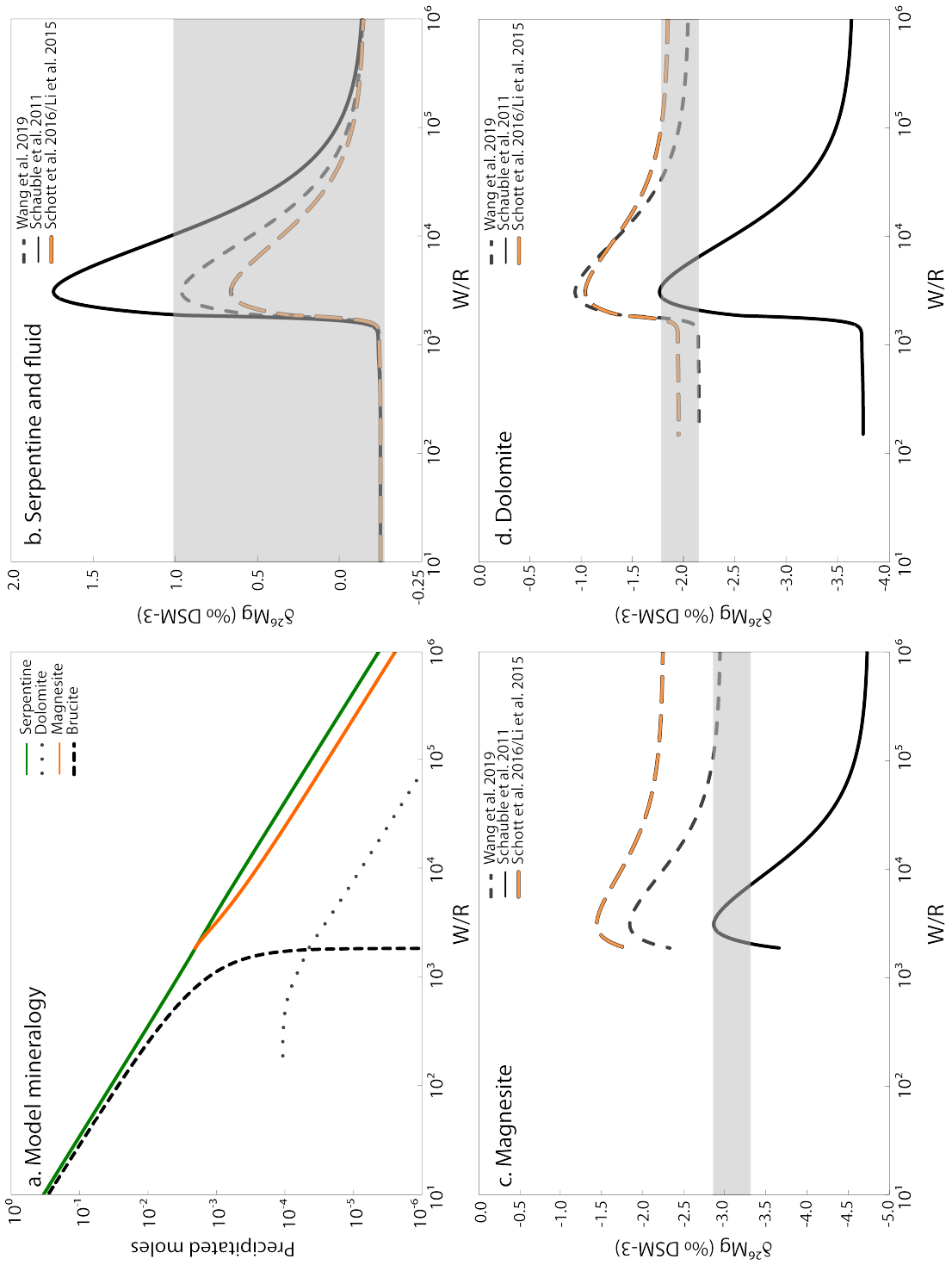

Figure 8. Results from the second stage of the reaction path model, closed to exchange with the atmosphere, illustrating mineral products (a), δ^{26}Mg of fluid and serpentine (b), magnesite (c), and dolomite (d). Grey squares illustrate the observed range of sample values for each mineral.

Given the range of model variables listed in Table 2, this model is able to explain three aspects of our Mg isotope data – 1) low δ^{26}Mg in massive carbonate veins, 2) high δ^{26}Mg in serpentine veins and some heavily weathered bulk rock samples, and 3) δ^{26}Mg of partially altered serpentinites that are indistinguishable from mantle values. The light values reflect co-precipitation of serpentine and carbonate at high W/R ratios. As W/R decreases, carbonates disappear from the crystallizing assemblage, the fluid evolves to δ^{26}Mg=-0.25‰, and precipitated serpentine also has mantle-like Mg isotope ratios, consistent with observed values in this and other studies (Beinlich et al., 2014; Liu et al., 2017). While the carbonate and serpentine samples in this study come from a broad region, and are not specifically co-genetic, our measurements show how serpentine veins can have magnesium isotopic ratios different from those of the protolith, even when serpentine-water exchange itself does not fractionate Mg-isotopes.

In the natural system, the Type II hyper-alkaline Ca-rich fluid comes in contact with the atmosphere in springs, where it combines with CO_2 from air to form extensive travertine deposits (Chavagnac et al., 2013a; Clark and Fontes, 1990; Kelemen et al., 2011; Kelemen and Matter, 2008; Mervine et al., 2014; Neal and Stanger, 1985). Travertines analyzed in this study have δ^{26}Mg of -1.14‰ and -0.89‰. In our modeling, at pH 12 the fluid has an isotope ratio identical to mantle values, δ^{26}Mg=-0.25‰. If calcite in travertines precipitated from this fluid, then the inferred $\Delta^{26}Mg_{cal\text{-}fl}$ of the travertine must have been lower than the value of ~3‰ expected for equilibrium fractionation with such a fluid (Li et al., 2012; Mavromatis et al., 2017; Wang et al., 2019). Indeed, Mavromatis et al. (2013) showed that $\Delta^{26}Mg_{cal\text{-}fl}$ is dependent on the growth rate of calcite, with $\Delta^{26}Mg_{cal\text{-}fl}$ ($\delta^{26}Mg_{cal} - \delta^{26}Mg_{fl}$) decreasing with increasing growth rate. (This type of growth rate dependence has not been reported for magnesite or dolomite). The inferred $\Delta^{26}Mg_{cal\text{-}fl}$ for calcite

in Oman travertines suggests calcite growth rates of ~ 10^{-5} mol/(m^2s). Such rapid growth is consistent with the non-equilibrium, high Mg contents in peridotite-hosted travertines in the Samail ophiolite and other massifs (e.g. Barnes and O'Neil, 1971, 1969; Chavagnac et al., 2013; Kelemen et al., 2011; Kelemen and Matter, 2008; Streit et al., 2012). Assuming that 1 to 10% of the total estimated travertine area in the Samail ophiolite (~10^7 m^2 (Kelemen and Matter, 2008)) is actively precipitating, this rate yields a total uptake of 10^3-10^4 tons atmospheric CO_2/yr, similar to previous estimates of carbon uptake to form travertine in the ophiolite (Kelemen et al., 2011; Kelemen and Matter, 2008; Mervine et al., 2014), as shown schematically in figure 9.

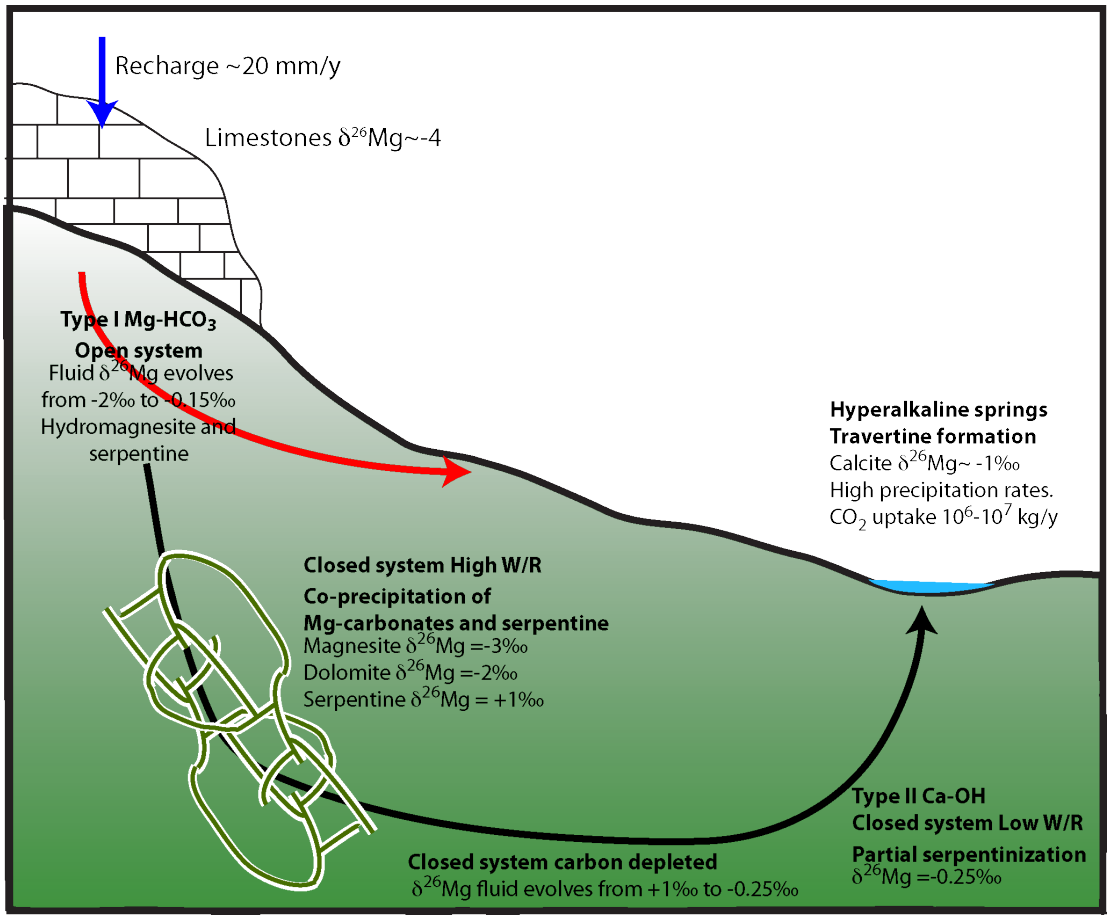

Figure 9. Conceptual model of Mg isotope systematics in the modern alteration system in Oman (after Dewandel et al., 2005; Neal and Stanger, 1985).

6. Conclusions

Most partially serpentinized dunites and harzburgites in the mantle section of the Samail ophiolite have δ^{26}Mg indistinguishable from average mantle values. Serpentinization at low W/R does not fractionate Mg isotopes. However, deviations from mantle δ^{26}Mg are observed in rocks which have undergone extensive Mg leaching at higher W/R. Heavily altered peridotites recording up to 30% Mg loss, and containing Mg-clay minerals, have the heaviest δ^{26}Mg ever reported for ultramafic rocks. We model a mechanism in which Mg-rich carbonates precipitate at high W/R, preferentially incorporating ^{24}Mg and producing ^{26}Mg-rich fluids that then precipitate serpentine veins with heavy Mg. When carbonates disappear from the crystallizing assemblage at lower W/R, serpentine evolves to mantle-like δ^{26}Mg. The modelled δ^{26}Mg for serpentine formed along with carbonates is similar to observed δ^{26}Mg in serpentine vein samples. The fact that most peridotite-hosted carbonate veins have finite ^{14}C ages, along with our modelling results, is consistent with other observations indicating that serpentinization and carbonation are ongoing in Oman. The proposed mechanism can be further explored using co-genetic carbonate-serpentine veins from the newly drilled cores from the Oman Drilling Project. δ^{26}Mg in calcite forming travertine deposits at peridotite-hosted alkaline springs is heavier than expected from equilibrium fractionation between calcite and fluid with mantle-like Mg isotope ratios, suggesting rapid, disequilibrium crystallization. We infer calcite growth rates of 10^{-5} mol/m^{2}s, corresponding to uptake of atmospheric CO_2 at a rate of 10^6-10^7 kg CO_2/yr to form travertine in Oman.

Acknowledgments

We thank everyone at the Sultanate of Oman Public Authority for Mining, especially Dr. Ali Al Rajhi for facilitating our fieldwork in Oman. This work was supported through the Sloan

Foundation – Deep Carbon Observatory (Grant 2014-3-01, Kelemen PI), the U.S.-National Science Foundation (NSF-EAR-1516300, Kelemen lead PI). All geochemical data for this work will be uploaded to PetDB (http://www.earthchem.org/petdb) and is included with the manuscript for the review process.

References

Al-Khirbash, S., 2016. Geology, mineralogy, and geochemistry of low grade Ni-lateritic soil (Oman Mountains, Oman). Chemie der Erde - Geochemistry. https://doi.org/10.1016/j.chemer.2016.08.002

Al-Khirbash, S., 2015. Genesis and mineralogical classification of Ni-laterites, Oman Mountains. Ore Geol. Rev. 65, 199–212. https://doi.org/10.1016/j.oregeorev.2014.09.022

Arvidson, R.S., Mackenzie, F.T., 1999. The dolomite problem; control of precipitation kinetics by temperature and saturation state. Am. J. Sci. 299, 257–288. https://doi.org/10.2475/ajs.299.4.257

Asimow, P.D., 1999. A model that reconciles major- and trace-element data from abyssal peridotites. Earth Planet. Sci. Lett. 169, 303–319. https://doi.org/10.1016/S0012-821X(99)00084-9

Auclair, M., Gauthier, M., Trottier, J., Jebrak, M., Chartrand, F., 1993. Mineralogy, geochemistry, and paragenesis of the Eastern Metals serpentinite-associated Ni-Cu-Zn deposit, Quebec Appalachians. Econ. Geol. 88, 123–138. https://doi.org/10.2113/gsecongeo.88.1.123

Baker, M.B., Beckett, J.R., 1999. The origin of abyssal peridotites: a reinterpretation of constraints based on primary bulk compositions. Earth Planet. Sci. Lett. 171, 49–61. https://doi.org/https://doi.org/10.1016/S0012-821X(99)00130-2

Barnes, I., LaMarche, V.C., Himmelberg, G., 1967. Geochemical Evidence of Present-Day Serpentinization. Science (80-.). 156, 830–832. https://doi.org/10.1126/science.156.3776.830

Barnes, I., O'Neil, J.R., 1971. Calcium-magnesium carbonate solid solutions from Holocene conglomerate cements and travertines in the Coast Range of California. Geochim. Cosmochim. Acta 35, 699–718. https://doi.org/10.1016/0016-7037(71)90068-8

Barnes, I., O'Neil, J.R., 1969. The Relationship between Fluids in Some Fresh Alpine-Type Ultramafics and Possible Modern Serpentinization, Western United States. Geol. Soc. Am. Bull. 80, 1947. https://doi.org/10.1130/0016-7606(1969)80[1947:TRBFIS]2.0.CO;2

Barnes, I., O'Neil, J.R., Trescases, J.., 1978. Present day serpentinization in New Caledonia, Oman and Yugoslavia. Geochim. Cosmochim. Acta 42, 144–145.

https://doi.org/10.1016/0016-7037(78)90225-9

Beinlich, A., Austrheim, H., Mavromatis, V., Grguric, B., Putnis, C. V., Putnis, A., 2018. Peridotite weathering is the missing ingredient of Earth's continental crust composition. Nat. Commun. 9. https://doi.org/10.1038/s41467-018-03039-9

Beinlich, A., Mavromatis, V., Austrheim, H., Oelkers, E.H., 2014. Inter-mineral Mg isotope fractionation during hydrothermal ultramafic rock alteration – Implications for the global Mg-cycle. Earth Planet. Sci. Lett. 392, 166–176. https://doi.org/10.1016/j.epsl.2014.02.028

Boudier, F., Coleman, R.G., 1981. Cross section through the peridotite in the Samail ophiolite, southeastern Oman Mountains. J. Geophys. Res. Solid Earth 86, 2573–2592. https://doi.org/10.1029/JB086iB04p02573

Braun, M.G., 2004. Petrologic and Microstructural Constraints on Focused Melt Transport in Dunites and Rheology of the Shallow Mantle. WHOI/MIT.

Braun, M.G., Kelemen, P.B., 2002. Dunite distribution in the Oman Ophiolite: Implications for melt flux through porous dunite conduits. Geochemistry, Geophys. Geosystems 3, 1–21. https://doi.org/10.1029/2001GC000289

Bruni, J., Canepa, M., Chiodini, G., Cioni, R., Cipolli, F., Longinelli, A., Marini, L., Ottonello, G., Vetuschi Zuccolini, M., 2002. Irreversible water–rock mass transfer accompanying the generation of the neutral, Mg–HCO3 and high-pH, Ca–OH spring waters of the Genova province, Italy. Appl. Geochemistry 17, 455–474. https://doi.org/10.1016/S0883-2927(01)00113-5

Chavagnac, V., Ceuleneer, G., Monnin, C., Lansac, B., Hoareau, G., Boulart, C., 2013a. Mineralogical assemblages forming at hyperalkaline warm springs hosted on ultramafic rocks: A case study of Oman and Ligurian ophiolites. Geochemistry, Geophys. Geosystems 14, 2474–2495. https://doi.org/10.1002/ggge.20146

Chavagnac, V., Monnin, C., Ceuleneer, G., Boulart, C., Hoareau, G., 2013b. Characterization of hyperalkaline fluids produced by low-temperature serpentinization of mantle peridotites in the Oman and Ligurian ophiolites. Geochemistry, Geophys. Geosystems 14, 2496–2522. https://doi.org/10.1002/ggge.20147

Clark, I.D., Fontes, J.-C., 1990. Paleoclimatic reconstruction in northern Oman based on carbonates from hyperalkaline groundwaters. Quat. Res. 33, 320–336. https://doi.org/10.1016/0033-5894(90)90059-T

Coleman, R.G., Keith, T.E., 1971. A Chemical Study of Serpentinization — Burro Moutain, California. J. Petrol. 12, 311–328.

Collier, M.L., 2012. Spatial-Statistical Properties of Geochemical Variability as Constraints on Magma Transport and Evolution Processes at Ocean Ridges. Columbia University.

de Obeso, J.C., Kelemen, P.B., 2020. Major element mobility during serpentinization, oxidation and weathering of mantle peridotite at low temperatures. Philos. Trans. A. Math. Phys. Eng. Sci. 378, 20180433. https://doi.org/10.1098/rsta.2018.0433

de Obeso, J.C., Kelemen, P.B., 2018. Fluid rock interactions on residual mantle peridotites overlain by shallow oceanic limestones: Insights from Wadi Fins, Sultanate of Oman. Chem. Geol. https://doi.org/10.1016/J.CHEMGEO.2018.09.022

DePaolo, D.J., 1981. Trace element and isotopic effects of combined wallrock assimilation and fractional crystallization. Earth Planet. Sci. Lett. 53, 189–202. https://doi.org/10.1016/0012-821X(81)90153-9

Esteban Guzman, J., Cuevas Urionabarrenechea, J., Tubía Martínez, J., Velasco Roldán, F., Vegas Tubia, N., 2011. Características petrográficas y mineralógicas de birbiritas derivadas de las peridotitas de Ronda (Cordilleras Béticas). Geogaceta 39–42.

Falk, E.S., Kelemen, P.B., 2015. Geochemistry and petrology of listvenite in the Samail ophiolite, Sultanate of Oman: Complete carbonation of peridotite during ophiolite emplacement. Geochim. Cosmochim. Acta 160, 70–90. https://doi.org/10.1016/j.gca.2015.03.014

Frost, R.B., 1985. On the stability of sulfides, oxides, and native metals in serpentinite. J. Petrol. 26, 31–63. https://doi.org/10.1093/petrology/26.1.31

Galy, A., Belshaw, N.S., Halicz, L., O'Nions, R.K., 2001. High-precision measurement of magnesium isotopes by multiple-collector inductively coupled plasma mass spectrometry. Int. J. Mass Spectrom. 208, 89–98. https://doi.org/10.1016/S1387-3806(01)00380-3

Galy, A., Yoffe, O., Janney, P.E., Williams, R.W., Cloquet, C., Alard, O., Halicz, L., Wadhwa, M., Hutcheon, I.D., Ramon, E., Carignan, J., 2003. Magnesium isotope heterogeneity of the isotopic standard SRM980 and new reference materials for magnesium-isotope-ratio measurements. J. Anal. At. Spectrom. 18, 1352–1356. https://doi.org/10.1039/B309273A

Gao, C., Cao, X., Liu, Q., Yang, Y., Zhang, S., He, Y., Tang, M., Liu, Y., 2018. Theoretical calculation of equilibrium Mg isotope fractionations between minerals and aqueous solutions. Chem. Geol. 488, 62–75. https://doi.org/10.1016/J.CHEMGEO.2018.04.005

Godard, M., Jousselin, D., Bodinier, J.-L., 2000. Relationships between geochemistry and structure beneath a palaeo-spreading centre: a study of the mantle section in the Oman ophiolite. Earth Planet. Sci. Lett. 180, 133–148. https://doi.org/10.1016/S0012-821X(00)00149-7

Gregory, R.T., Taylor, H.P., 1981. An Oxygen Isotope Profile in a Section of Cretaceous Oceanic Crust, Samail Ophiolite, Oman: Evidence for δ18O Buffering of the Oceans Circulation at Mid-Ocean Ridges. J. Geophys. Res. 86, 2737–2755.

Hänchen, M., Prigiobbe, V., Baciocchi, R., Mazzotti, M., 2008. Precipitation in the Mg-carbonate system—effects of temperature and CO2 pressure. Chem. Eng. Sci. 63, 1012–1028. https://doi.org/10.1016/J.CES.2007.09.052

Hanghøj, K., Kelemen, P.B., Hassler, D., Godard, M., 2010. Composition and Genesis of Depleted Mantle Peridotites from the Wadi Tayin Massif, Oman Ophiolite; Major and Trace Element Geochemistry, and Os Isotope and PGE Systematics. J. Petrol. 51, 201–227. https://doi.org/10.1093/petrology/egp077

Higgins, J.A., Schrag, D.P., 2010. Constraining magnesium cycling in marine sediments using magnesium isotopes. Geochim. Cosmochim. Acta 74, 5039–5053. https://doi.org/10.1016/j.gca.2010.05.019

Hotz, P.E., 1964. Nickeliferous laterites in southwestern Oregon and northwestern California. Econ. Geol. 59, 355–396. https://doi.org/10.2113/gsecongeo.59.3.355

Husson, J.M., Higgins, J.A., Maloof, A.C., Schoene, B., 2015. Ca and Mg isotope constraints on the origin of Earth's deepest δ13C excursion. Geochim. Cosmochim. Acta 160, 243–266. https://doi.org/10.1016/j.gca.2015.03.012

Jagoutz, E., Palme, H., Baddenhausen, H., Blum, K., Cendales, M., Dreibus, G., Spettel, B., Lorenz, V., Wanke, H., 1979. The abundances of major, minor and trace elements in the earth's mantle as derived from primitive ultramafic nodules, in: Proceedings of the Lunar and Planetary Science Conference 10. pp. 2031–2050.

Johnson, N.C., Thomas, B., Maher, K., Rosenbauer, R.J., Bird, D., Brown, G.E., 2014. Olivine dissolution and carbonation under conditions relevant for in situ carbon storage. Chem. Geol. 373, 93–105. https://doi.org/10.1016/J.CHEMGEO.2014.02.026

Kelemen, P.B., de Obeso, J.C., Manning, C., Godard, M., Bach, W., Cai, Y., Choe, S., Coggon, J., Ellison, E., Eslami, A., Evans, K., Harris, M., Kahl, W.-A., Matter, J., Michibayashi, K., Okazaki, K., Pezard, P., Teagle, D., Templeton, A., OmanDP Science Team, Team, O.S., 2019. Peridotite alteration in OmanDP cores, in: Geophysical Research Abstracts. pp. EGU2019-17259.

Kelemen, P.B., Matter, J.M., 2008. In situ carbonation of peridotite for CO2 storage. Proc. Natl. Acad. Sci. 105, 17295–17300. https://doi.org/10.1073/pnas.0805794105

Kelemen, P.B., Matter, J.M., Streit, E.E., Rudge, J.F., Curry, W.B., Blusztajn, J., 2011. Rates and Mechanisms of Mineral Carbonation in Peridotite: Natural Processes and Recipes for Enhanced, in situ CO 2 Capture and Storage. Annu. Rev. Earth Planet. Sci. 39, 545–576. https://doi.org/10.1146/annurev-earth-092010-152509

Kelemen, P.B., Matter, J.M., Teagle, D.A.H., Coggon, J.A. (Eds.), 2020. Proceedings of the Oman Drilling Project, Proceedings of the International Ocean Discovery Program. International Ocean Discovery Program. https://doi.org/10.14379/OmanDP.proc.2020

Land, L., 1998. Failure to Precipitate Dolomite at 25° C from Dilute Solution Despite 1000-Fold Oversaturation after 32 Years. Aquat. Geochemistry 361–368.

Li, W., Beard, B.L., Li, C., Xu, H., Johnson, C.M., 2015. Experimental calibration of Mg isotope fractionation between dolomite and aqueous solution and its geological implications. Geochim. Cosmochim. Acta 157, 164–181.

Li, W., Chakraborty, S., Beard, B.L., Romanek, C.S., Johnson, C.M., 2012. Magnesium isotope fractionation during precipitation of inorganic calcite under laboratory conditions. Earth Planet. Sci. Lett. 333–334, 304–316. https://doi.org/10.1016/J.EPSL.2012.04.010

Liu, P.-P., Teng, F.-Z., Dick, H.J.B., Zhou, M.-F., Chung, S.-L., 2017. Magnesium isotopic composition of the oceanic mantle and oceanic Mg cycling. Geochim. Cosmochim. Acta 206, 151–165. https://doi.org/10.1016/j.gca.2017.02.016

Lorand, J.P., 1988. Fe□Ni□Cu sulfides in tectonite peridotites from the Maqsad district, Sumail ophiolite, southern Oman: Implications for the origin of the sulfide component in the oceanic upper mantle. Tectonophysics 151, 57–73. https://doi.org/10.1016/0040-1951(88)90240-5

Malvoisin, B., 2015. Mass transfer in the oceanic lithosphere: Serpentinization is not isochemical. Earth Planet. Sci. Lett. 430, 75–85. https://doi.org/10.1016/j.epsl.2015.07.043

Mavromatis, V., Gautier, Q., Bosc, O., Schott, J., 2013. Kinetics of Mg partition and Mg stable isotope fractionation during its incorporation in calcite. Geochim. Cosmochim. Acta 114, 188–203. https://doi.org/10.1016/J.GCA.2013.03.024

Mavromatis, V., Purgstaller, B., Dietzel, M., Buhl, D., Immenhauser, A., Schott, J., 2017. Impact of amorphous precursor phases on magnesium isotope signatures of Mg-calcite. Earth Planet. Sci. Lett. 464, 227–236. https://doi.org/10.1016/J.EPSL.2017.01.031

Mervine, E.M., Humphris, S.E., Sims, K.W.W., Kelemen, P.B., Jenkins, W.J., 2014. Carbonation rates of peridotite in the Samail Ophiolite, Sultanate of Oman, constrained through 14C dating and stable isotopes. Geochim. Cosmochim. Acta 126, 371–397. https://doi.org/10.1016/j.gca.2013.11.007

Monnier, C., Girardeau, J., Le Mée, L., Polvé, M., 2006. Along-ridge petrological segmentation of the mantle in the Oman ophiolite. Geochemistry, Geophys. Geosystems 7, n/a-n/a. https://doi.org/10.1029/2006GC001320

Monnin, C., Chavagnac, V., Ceuleneer, G., Boulart, C., Hoareau, G., 2011. Characterization of hyperalkaline fluids produced by serpentinization of mantle peridotites in Oman and in Liguria (Northern Italy). Mineral. Mag 75, 1490.

Moody, J.B., 1976. Serpentinization: a review. Lithos 9, 125–138. https://doi.org/10.1016/0024-4937(76)90030-X

Nasir, S., Al Sayigh, A.R., Al Harthy, A., Al-Khirbash, S., Al-Jaaidi, O., Musllam, A., Al-Mishwat, A., Al-Bu'saidi, S., 2007. Mineralogical and geochemical characterization of listwaenite from the Semail Ophiolite, Oman. Chemie der Erde - Geochemistry 67, 213–228. https://doi.org/10.1016/j.chemer.2005.01.003

Neal, C., Stanger, G., 1985. Past and present serpentinization of ultramafic rocks: An example from the Semail ophiolite nappe of northern Oman, in: Drewer, J. (Ed.), The Chemistry of Weathering. D. Reidel Publishing Company, Dordrecht, Holland, pp. 249–275.

Neal, C., Stanger, G., 1983. Hydrogen generation from mantle source rocks in Oman. Earth Planet. Sci. Lett. 66, 315–320. https://doi.org/10.1016/0012-821X(83)90144-9

Noël, J., Godard, M., Oliot, E., Martinez, I., Williams, M., Boudier, F., Rodriguez, O., Chaduteau, C., Escario, S., Gouze, P., 2018. Evidence of polygenetic carbon trapping in the Oman Ophiolite: Petro-structural, geochemical, and carbon and oxygen isotope study of the Wadi Dima harzburgite-hosted carbonates (Wadi Tayin massif, Sultanate of Oman). Lithos 323, 218–237. https://doi.org/10.1016/J.LITHOS.2018.08.020

Oelkers, E.H., Berninger, U.N., Pérez-Fernàndez, A., Chmeleff, J., Mavromatis, V., 2018. The temporal evolution of magnesium isotope fractionation during hydromagnesite dissolution, precipitation, and at equilibrium. Geochim. Cosmochim. Acta 226, 36–49. https://doi.org/10.1016/j.gca.2017.11.004

Oskierski, H.C., Beinlich, A., Mavromatis, V., Altarawneh, M., Dlugogorski, B.Z., 2019. Mg isotope fractionation during continental weathering and low temperature carbonation of ultramafic rocks. Geochim. Cosmochim. Acta 262, 60–77. https://doi.org/10.1016/J.GCA.2019.07.019

Paukert, A.N., Matter, J.M., Kelemen, P.B., Shock, E.L., Havig, J.R., 2012. Reaction path

modeling of enhanced in situ CO2 mineralization for carbon sequestration in the peridotite of the Samail Ophiolite, Sultanate of Oman. Chem. Geol. 330–331, 86–100. https://doi.org/10.1016/j.chemgeo.2012.08.013

Pearce, C.R., Saldi, G.D., Schott, J., Oelkers, E.H., 2012. Isotopic fractionation during congruent dissolution, precipitation and at equilibrium: Evidence from Mg isotopes. Geochim. Cosmochim. Acta 92, 170–183. https://doi.org/10.1016/j.gca.2012.05.045

Pinilla, C., Blanchard, M., Balan, E., Natarajan, S.K., Vuilleumier, R., Mauri, F., 2015. Equilibrium magnesium isotope fractionation between aqueous Mg2+ and carbonate minerals: Insights from path integral molecular dynamics. Geochim. Cosmochim. Acta 163, 126–139. https://doi.org/10.1016/j.gca.2015.04.008

Power, I.M., Kenward, P.A., Dipple, G.M., Raudsepp, M., 2017. Room Temperature Magnesite Precipitation. Cryst. Growth Des. 17, 5652–5659. https://doi.org/10.1021/acs.cgd.7b00311

Ryu, J.-S., Vigier, N., Decarreau, A., Lee, S.-W., Lee, K.-S., Song, H., Petit, S., 2016. Experimental investigation of Mg isotope fractionation during mineral dissolution and clay formation. Chem. Geol. 445, 135–145. https://doi.org/10.1016/j.chemgeo.2016.02.006

Saldi, G.D., Schott, J., Pokrovsky, O.S., Gautier, Q., Oelkers, E.H., 2012. An experimental study of magnesite precipitation rates at neutral to alkaline conditions and 100–200 °C as a function of pH, aqueous solution composition and chemical affinity. Geochim. Cosmochim. Acta 83, 93–109. https://doi.org/10.1016/J.GCA.2011.12.005

Santiago Ramos, D.P., Coogan, L.A., Murphy, J.G., Higgins, J.A., 2020. Low-temperature oceanic crust alteration and the isotopic budgets of potassium and magnesium in seawater. Earth Planet. Sci. Lett. 541, 116290. https://doi.org/10.1016/j.epsl.2020.116290

Schauble, E.A., 2011. First-principles estimates of equilibrium magnesium isotope fractionation in silicate, oxide, carbonate and hexaaquamagnesium(2+) crystals. Geochim. Cosmochim. Acta 75, 844–869. https://doi.org/10.1016/J.GCA.2010.09.044

Schott, J., Mavromatis, V., Fujii, T., Pearce, C.R., Oelkers, E.H., 2016. The control of carbonate mineral Mg isotope composition by aqueous speciation: Theoretical and experimental modeling. Chem. Geol. 445, 120–134. https://doi.org/10.1016/j.chemgeo.2016.03.011

Shirokova, L.S., Mavromatis, V., Bundeleva, I.A., Pokrovsky, O.S., Bénézeth, P., Gérard, E., Pearce, C.R., Oelkers, E.H., 2013. Using Mg Isotopes to Trace Cyanobacterially Mediated Magnesium Carbonate Precipitation in Alkaline Lakes. Aquat. Geochemistry 19, 1–24. https://doi.org/10.1007/s10498-012-9174-3

Skarpelis, N., 2006. Lateritization processes of ultramafic rocks in Cretaceous times: The fossil weathering crusts of mainland Greece. J. Geochemical Explor. 88, 325–328. https://doi.org/10.1016/j.gexplo.2005.08.066

Snow, J.E., Dick, H.J.B., 1995. Pervasive magnesium loss by marine weathering of peridotite. Geochim. Cosmochim. Acta 59, 4219–4235. https://doi.org/10.1016/0016-7037(95)00239-V

Stanger, G., 1985. Silicified serpentinite in the Semail nappe of Oman. Lithos 18, 13–22. https://doi.org/10.1016/0024-4937(85)90003-9

Streit, E., Kelemen, P.B., Eiler, J., 2012. Coexisting serpentine and quartz from carbonate-

bearing serpentinized peridotite in the Samail Ophiolite, Oman. Contrib. to Mineral. Petrol. 164, 821–837. https://doi.org/10.1007/s00410-012-0775-z

Su, B.-X., Teng, F.-Z., Hu, Y., Shi, R.-D., Zhou, M.-F., Zhu, B., Liu, F., Gong, X.-H., Huang, Q.-S., Xiao, Y., Chen, C., He, Y.-S., 2015. Iron and magnesium isotope fractionation in oceanic lithosphere and sub-arc mantle: Perspectives from ophiolites, Earth and Planetary Science Letters. https://doi.org/10.1016/j.epsl.2015.08.020

Teng, F.-Z., 2017. Magnesium Isotope Geochemistry. Rev. Mineral. Geochemistry 82, 219–287. https://doi.org/10.2138/rmg.2017.82.7

Teng, F.-Z., Li, W.-Y., Ke, S., Marty, B., Dauphas, N., Huang, S., Wu, F.-Y., Pourmand, A., 2010. Magnesium isotopic composition of the Earth and chondrites. Geochim. Cosmochim. Acta 74, 4150–4166. https://doi.org/10.1016/j.gca.2010.04.019

Teng, F.Z., Li, W.Y., Ke, S., Yang, W., Liu, S.A., Sedaghatpour, F., Wang, S.J., Huang, K.J., Hu, Y., Ling, M.X., Xiao, Y., Liu, X.M., Li, X.W., Gu, H.O., Sio, C.K., Wallace, D.A., Su, B.X., Zhao, L., Chamberlin, J., Harrington, M., Brewer, A., 2015. Magnesium Isotopic Compositions of International Geological Reference Materials. Geostand. Geoanalytical Res. 39, 329–339. https://doi.org/10.1111/j.1751-908X.2014.00326.x

Tipper, E.T.T., Galy, A., Gaillardet, J., Bickle, M.J.J., Elderfield, H., Carder, E.A.A., 2006. The magnesium isotope budget of the modern ocean: Constraints from riverine magnesium isotope ratios. Earth Planet. Sci. Lett. 250, 241–253. https://doi.org/10.1016/j.epsl.2006.07.037

Wang, W., Zhou, C., Liu, Y., Wu, Z., Huang, F., 2019. Equilibrium Mg isotope fractionation among aqueous Mg2+, carbonates, brucite and lizardite: Insights from first-principles molecular dynamics simulations. Geochim. Cosmochim. Acta 250, 117–129. https://doi.org/10.1016/J.GCA.2019.01.042

Weyhenmeyer, C.E., Burns, S.J., Waber, H.N., Matter, A., 2002. Isotope study of moisture sources , recharge areas , and groundwater flow paths within the eastern Batinah coastal plain , Sultanate of Oman 38, 1–22. https://doi.org/10.1029/2000WR000149

Wimpenny, J., Colla, C.A., Yin, Q.-Z.Z., Rustad, J.R., Casey, W.H., 2014. Investigating the behaviour of Mg isotopes during the formation of clay minerals. Geochim. Cosmochim. Acta 128, 178–194. https://doi.org/10.1016/j.gca.2013.12.012

Wimpenny, J., Gíslason, S.R., James, R.H., Gannoun, A., Pogge Von Strandmann, P.A.E., Burton, K.W., 2010. The behaviour of Li and Mg isotopes during primary phase dissolution and secondary mineral formation in basalt. Geochim. Cosmochim. Acta 74, 5259–5279. https://doi.org/10.1016/j.gca.2010.06.028

Young, E.D., Galy, A., 2004. The Isotope Geochemistry and Cosmochemistry of Magnesium. Rev. Mineral. Geochemistry 55, 197 LP – 230.

JGR: Solid Earth

Supporting Information for

A Mg isotopic perspective on the mobility of magnesium during serpentinization and carbonation of the Oman ophiolite

Juan Carlos de Obeso[1*], Danielle P. Santiago Ramos[2^], John A. Higgins[2], Peter B. Kelemen[3]

[1] Lamont Doherty Earth Observatory, Columbia University, Palisades, NY, USA

[2] Department of Geosciences, Princeton University, Princeton, NJ, USA

[3] Dept. of Earth & Environmental Sciences, Columbia University, Lamont Doherty Earth Observatory, Palisades, NY, USA

^ now at Geology & Geophysics, Woods Hole Oceanographic Institution, Wood Hole, MA, USA

Contents of this file

Tables S1 to S3

Additional Supporting Information (Files uploaded separately)

Captions for Tables S1 to S3 (if larger than 1 page, upload as separate file)

Introduction

We present as supplementary tables details on the major element composition of new samples as well as details of the calibration used during ICP-OES run. We also included a table of magnesium isotopic compositions of USGS standards measured as unknowns with this study samples.

Table S1. Major element composition of serpentinite, serpentine and carbonates veins from the Samail ophiolite

Table S2. Standards used for ICP-OES calibration

Table S3. Mg isotope composition measured for USGS rock standards